Hindawi
Advances in Materials Science and Engineering
Volume 2018, Article ID 5241848, 10 pages
https://doi.org/10.1155/2018/5241848

Research Article

Experimental Study on the Tensile Properties of Rock-Mortar Interface under Different Strain Rates

Nan Wu,[1,2] **Zhende Zhu**,[1,2] **and Zhilei He**[1,2]

[1]*Key Laboratory of Ministry of Education for Geomechanics and Embankment Engineering, Hohai University, Nanjing 210098, China*
[2]*Jiangsu Research Center for Geotechnical Engineering Technology, Hohai University, Nanjing 210098, China*

Correspondence should be addressed to Nan Wu; wunanhhu@hhu.edu.cn

Received 14 April 2018; Accepted 2 August 2018; Published 3 September 2018

Academic Editor: Aniello Riccio

In this paper, an experimental study was carried out on a rock-mortar interface specimen under three different strain rates (10^{-6}, 10^{-5}, and 10^{-4} s^1) using the MTS322 electrohydraulic servo loading system, and a new constitutive relation function of fictitious crack model (FCM) according to the axial-stress-crack-width curves of the rock-mortar interface is established, because the traditional nonlinear softening function easily distorts, shakes, and so cannot describe the damage-evolution process of the rock-mortar interface accurately. Through the use of a precise servo actuator system and three extensometers measured axial-stress-crack-width curves, it is shown that the rock-mortar interface is very sensitive to the strain rate. The tensile strength increases with strain rate, the crack width decreases at the same time, and the axial-stress-crack-width curves gradually evolve from a concave-downward trend to a linear decreasing trend. At the same time, the new constitutive relation function can reflect the tensile strength, crack width, and the downward trend of the rock-mortar interface more accurately.

1. Introduction

The interface between rock and mortar in the project often becomes the weakest point of the entire project, and thus research in this area is of great significance. Owing to the structural characteristics of rock and concrete itself, which usually act as the compression material in most structures, the compressive strain rate accounts for a large subfield in the study of rock and concrete material properties under different strain rates. However, the different strain rates' tensile stress in the actions of explosions and earthquakes cannot be avoided. In the Great Hanshin-Awaji earthquake, some special damage in building structures were likely caused by interface tensile stress wave propagation [1].

However, the dynamic tensile has not been widely investigated, and there are few papers describing direct tensile test of the different strain rates in particular [2, 3]. This is because the direct tensile test is difficult, the equipment requires high precision and cannot achieve easily. It is believed that the tensile strength is approximately proportional to the square root of the compressive strength [3]. But a survey of the technical literature indicates wide scatter in tensile strength data. To date, the research on the axial tensile test of rock-mortar interface is very rare [4]. Yan et al. studied the dynamic tensile strength property of the rock interface and its host rocks sampled using split-Hopkinson pressure bar (SHPB) tests [5]. It was reported that the dynamic tensile strengths of the two host rocks, that is, tuff and basalt, have typical loading-rate dependency. However, the dynamic response of the rock interface is much more complicated and varies between those of tuff and basalt when the loading rate is given. Similar works and test results were also reported [6–9].

In order to further study the principle of this phenomenon, Hillerborg found that a large number of microcracks appear in the crack front and the surrounding area before overall instability of the material occurs and that the macrocracks always appear after these microcracks. Based on this, the fictitious crack model (FCM), which applied to describe the nonlinear behavior of brittle materials, was proposed by Hillerborg et al. [10]. Reinhardt et al. presented a nonlinear softening function to describe the

constitutive relation [11]. In some experiments, correct results can be obtained by fitting the experimental data with the nonlinear softening function.

The goal of this paper is to research the rock-mortar interface constitutive relation under different strain rate (10^{-6}, 10^{-5}, and 10^{-4} s^{-1}) using the MTS322 electro-hydraulic servo loading system. Through use of the direct tensile test method to obtain more accurate and reliable data, we propose a new constitutive relation function for fictitious crack model (FCM) and explore the changing trends of tensile strength, crack width, and downward trend with strain rate.

2. Experimental Studies

2.1. Materials and Test Specimens. Cylinder core samples were drilled from granite with a circular diameter (ϕ) of 74 mm, and both ends were rubbed until they become smooth and made lengthwise perpendicular by a cutting machine. The specimens were fabricated to $\phi 74 \times 150$ mm, and both ends were glued onto a steel plate with modified epoxy resin adhesive. The specimen was first tensioned on the MTS322 electro-hydraulic servo loading system until fracture destruction. Figure 1(a) shows the natural fracture surface. The fractured specimen was soaked and rinsed in water, then wrapped by plastic packaging on the flank of the cylinder, with the natural fracture surface toward the interior, and then fixed by an adhesive tape [4]. The strength of the plastic package ensures that the sample will not warp and deform during subsequent operations. The cement mortar, which has a mixing weight ratio of 0.5/1/2 (water/cement/sand), was then placed vertically on the fractured specimen, and then the specimen was vibrocompacted on the vibration table as shown in Figure 1(b). This experiment did not explore the correlation of the strain rate of the interfacial specimen and the mortar ratios. From the existing engineering practice, it is found that the mortar ratio in this experiment has a wide range of applications and representative and is thus chosen in this experiment. After maintaining for more than 28 d, the laitance was cut off, and the ends of the mortar were polished. Both ends of the specimen were then glued onto the steel plate (which had a screw hole in the center) with modified epoxy resin adhesive, and prepared for the tensile test, as shown in Figure 1(c).

Since each sample is made of rock and mortar, the elastic modulus of both under different strain rates adopts the secant modulus of the linear segment before peak at a strain value of 50 $\mu\varepsilon$, as shown in Figure 2. Many papers have shown the modulus of elasticity without significant change, only minor growth with increasing strain rate , represented as the linear growth trend [12, 13]. Rock material has similar properties, so the elastic modulus value when the strain rate is 10^{-5} s^{-1} adopts the mean value of the former two values. Other physical and mechanical parameters associated with the specimen and the elastic modulus of rock and mortar under different strain rates are shown in Table 1.

2.2. Test Equipment and Methods. The primary test equipment was a MTS322 electro-hydraulic servo loading system. An extensometer (MTS Systems Corp., Eden Prairie, MN, USA) was used to measure the displacement during experiments as shown in Figure 3. The extensometer's gauge length is 25 mm, and its measurement range is ±2.5 mm.

Each specimen is attached to the three-group extensometer-fixed frame with epoxy resin adhesive; the distance between the fixed frame and steel column is approximately 0.8–1 cm. The two ends of each specimen are connected to a ball joint by screws in the center of the steel cap, and the ball joint is connected to the fixture of the experimental equipment. The accuracy requirements for testing are met during the experiment by adjusting the tightness between the specimen and equipment and the state of the ball joint before loading. The test was conducted under conditions of three loading rates, 10^{-6}, 10^{-5}, and 10^{-4} s^{-1}. There were at least three specimens containing an interface comprising rock and mortar at every loading rate.

2.3. Test Results and Analysis. The fictitious crack model (FCM) regards as cracks begin, extension and polymerization, when stress achieved peak strength, and this process has not happened before peak strength [10]. The axial-stress-displacement curves of the rock-mortar samples under different strain rates are shown in Figures 4(a)–4(c). In rock-mortar interface specimens, with the natural fracture surface of rocks, each specimen section has its own independent characteristics. The shape of fractures and the area of fracture surfaces lead to the difference of bonding area between rock and mortar directly.

However, this does not affect the applicability of the FCM model. During the cracking of the specimen, the coalescence direction of the new cracks and the existing cracks is random and the stress distribution in the strain-softening area of the material is irregularly in the radial direction. Therefore, the final fracture surface of the specimen is not a smooth plane. However, the fictitious crack model (FCM) is a model that describes the constitutive relation from the macrodescription of the phenomenon. The model assumes that all tensile stresses on the bonded surface are consistent, and the tension is equivalent to the force on the projected area. This accords with the application foundation of FCM theory.

With increasing strain rate, the peak strength of the rock-mortar samples increases, and the overall deformation of the sample decreases gradually, as shown in Figures 4(a)–4(c) and Table 1. As the strain rate increases from 10^{-6} to 10^{-5} and 10^{-4} s^{-1}, the mean peak stress corresponding increases by 26.2% and 40.6%, respectively, and the corresponding deformation at the peak stress gradually decreases. Severe fluctuations and nonstop fluctuation of the stress may occur at the beginning of the peak, as shown at point 1 in Figure 4(b). This occurs because, due to different physical parameters, such as the elastic modulus and Poisson's ratio of the rock and mortar, and owing to the existence of large number of microcracks around the interface, when the peak strength is reached one or several microcracks develop quickly, and making the displacement increase suddenly, which leads to a sudden drop of the pull on the extensometer.

(a) (b) (c)

Figure 1: Fabrication process for rock-mortar interface specimen. (a) Natural fracture of rock; (b) casting of rock-mortar interface; (c) final rock-mortar interface specimen.

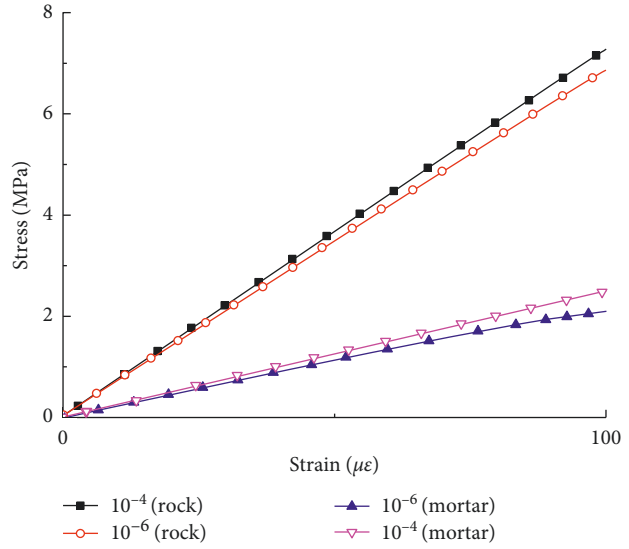

Figure 2: Stress-strain curve of rock-mortar interface under different strain rates.

Table 1: Parameters of rock-mortar interface specimen in direct tension test.

Sample label	Strain rate (s^{-1})	Elastic modulus (GPa)		Peak strength (MPa)	Crack width (mm)	The number of data points (–)
		Rock	Mortar			
DT-A-1	10^{-6}	56.5	18.7	2.14	0.145	7499
DT-A-2	10^{-6}	56.5	18.7	1.94	0.128	7005
DT-A-3	10^{-6}	56.5	18.7	1.98	0.140	6089
DT-B-1	10^{-5}	62	19.3	2.59	0.091	4193
DT-B-2	10^{-5}	62	19.3	2.38	0.086	9333
DT-B-3	10^{-5}	62	19.3	2.68	0.0950	7389
DT-C-1	10^{-4}	67.4	19.9	2.73	0.0225	1611
DT-C-2	10^{-4}	67.4	19.9	2.99	0.0218	2671
DT-C-3	10^{-4}	67.4	19.9	2.79	0.0221	2395

3. The Constitutive Relation Research

3.1. Traditional Nonlinear Softening Function. As shown in Figure 5, which depicts the direct tension test of the rock-mortar sample, the axial-stress-deformation curve of the sample is composed of five parts:

$$\delta = \delta_{ro} + \delta_{mo} + \omega + \delta_{re} + \delta_{me}, \quad (1)$$

where δ_{ro} is the residual deformation of the rock, δ_{mo} is the residual deformation of the mortar, ω is the crack width, δ_{re} is the elastic deformation of the rock, and δ_{me} is the elastic deformation of the mortar.

The residual deformation of the rock δ_{ro} is

$$\delta_{ro} = \delta_{rp} - \delta_{rep}, \quad (2)$$

where δ_{rp} is the total deformation at peak on the axial-stress-deformation curve and δ_{rep} is the elastic deformation of the rock part at peak on the axial-stress-deformation curve.

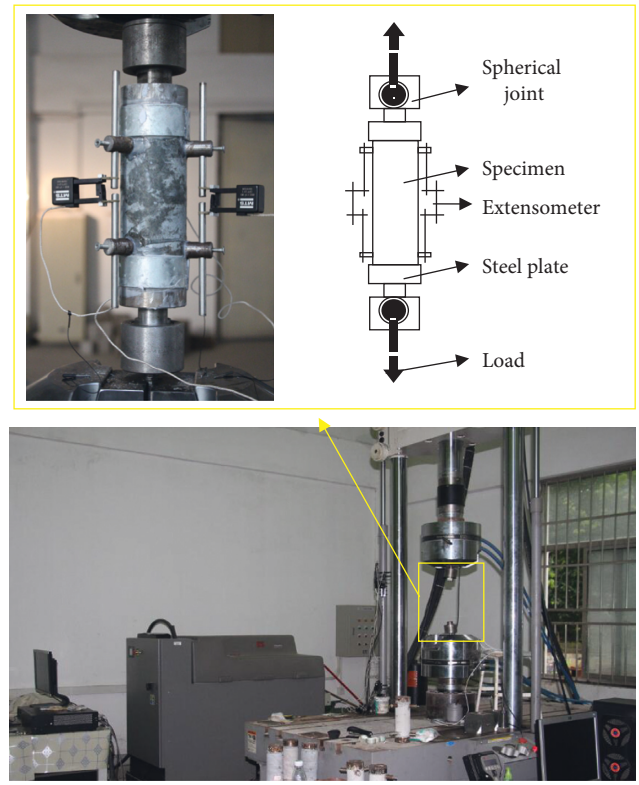

Figure 3: Extensometer of MTS322 electrohydraulic servoloading system.

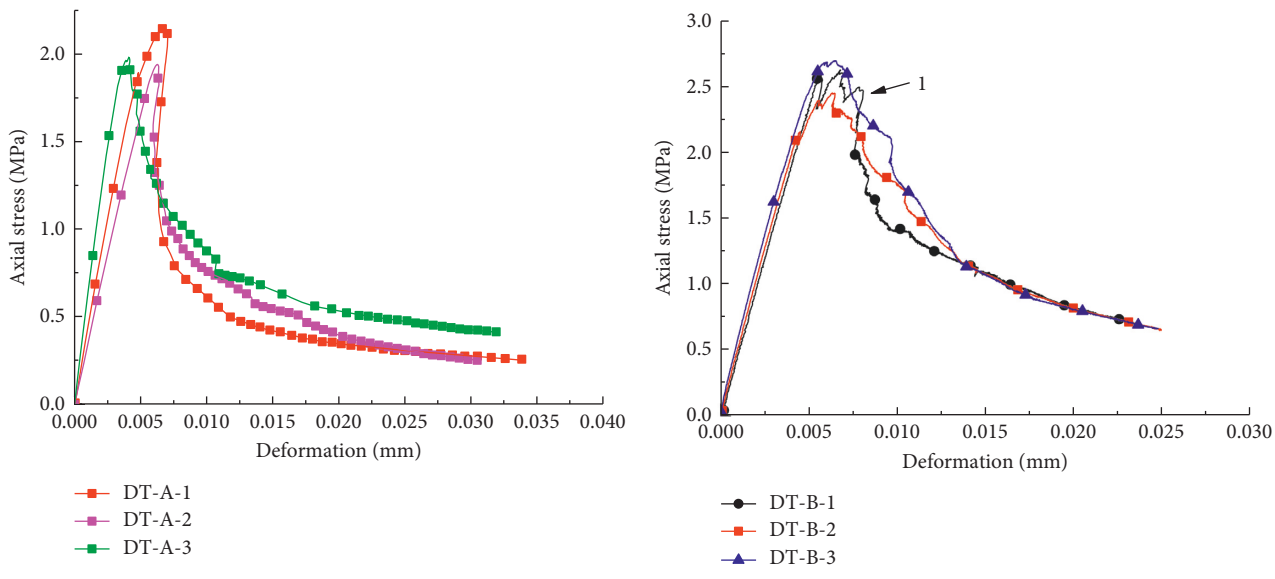

Figure 4: Continued.

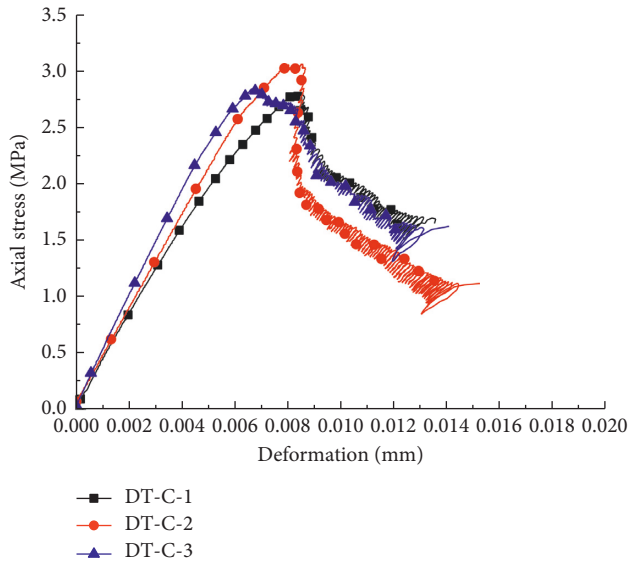

(c)

Figure 4: Axial-stress-deformation curves under different strain rates by experimental. (a) 10^{-6} s^{-1}; (b) 10^{-5} s^{-1}; (c) 10^{-4} s^{-1}.

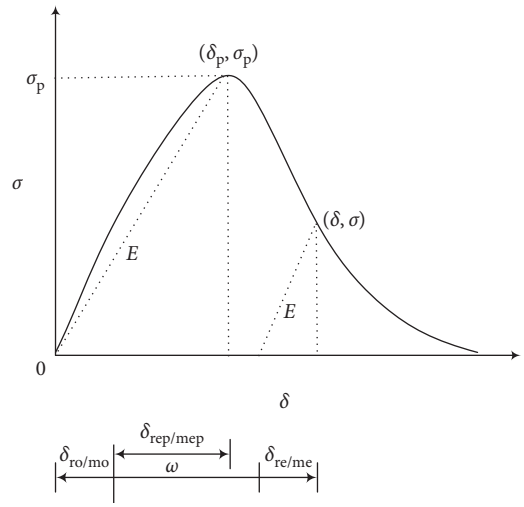

Figure 5: Schematic of axial-stress-deformation curves.

The residual deformation of the mortar δ_{mo} is

$$\delta_{mo} = \delta_{mp} - \delta_{mep}, \tag{3}$$

where δ_{mp} is the total deformation at peak on the axial-stress-deformation curve and δ_{mep} is the elastic deformation of the mortar part at peak on the axial-stress-deformation curve.

The formula for calculating the elastic deformation of rock (δ_{re}) is

$$\delta_{re} = \frac{\sigma l_r}{E_r}. \tag{4}$$

And that for calculating the elastic deformation of mortar (δ_{me}) is

$$\delta_{me} = \frac{\sigma l_m}{E_m}, \tag{5}$$

where l_r and l_m are the lengths of the rock and mortar parts of the sample, respectively, σ is the stress at some point, and E_r and E_m are the elastic moduli of the rock and mortar, respectively.

So the crack width (ω) can be obtained as follows:

$$\omega = \delta - \delta_{ro} - \delta_{mo} - \delta_{re} - \delta_{me}. \tag{6}$$

The length of the rock and mortar section of each specimen was measured before the test (l_r and l_m). The physicomechanical parameters of these two sections were also obtained in the previous tests, as shown in

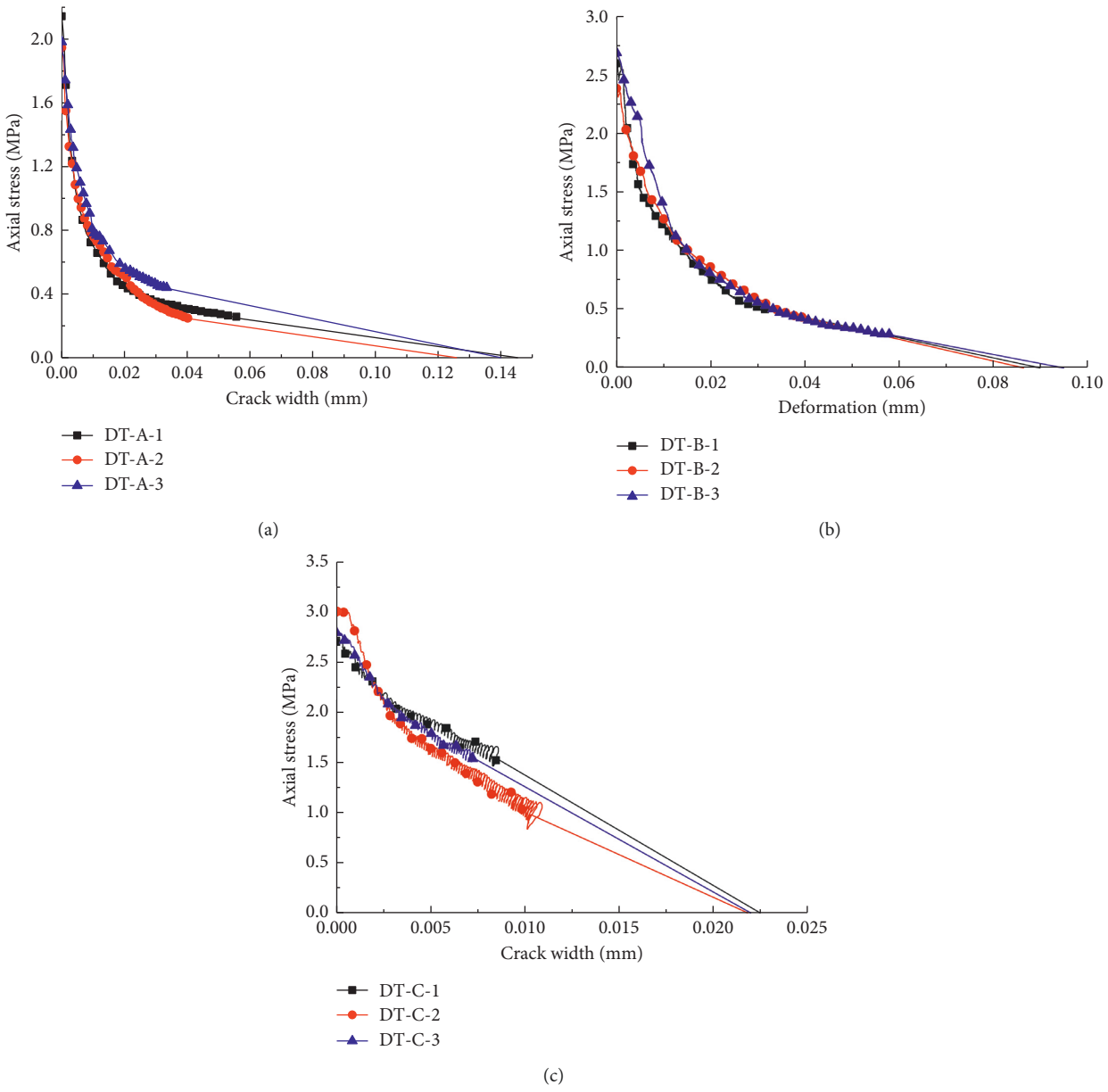

Figure 6: Axial-stress-crack-width curves under different strain rates ($\sigma - \omega$) by experimental. (a) 10^{-6} s^{-1}; (b) 10^{-5} s^{-1}; (c) 10^{-4} s^{-1}.

Table 1. During the process of axial tensile test, the overall deformation of the sample was measured by the extensometer, and the value of the elastic deformation and plastic deformation of the rock section and mortar section of each specimen was obtained by Equation (2)–Equation (5); the axial-stress-crack-width curves for different strain rates (10E-4, 10E-5, and 10E-6) were obtained, as shown in Figures 6(a)–6(c). As can be seen from these figures, along with increasing strain rate, the axial tensile strength of the rock-mortar interface increases and the maximum crack width decreases constantly. The axial-stress-crack-width curve varies from a concave-downward trend to a linearly decreasing trend.

Because the actual axial-stress-crack-width curve is a complex smooth curve, in order to make the FCM more easily applied to fracture process analysis, many scholars have presented a variety of simplified forms of the function expression. Reinhardt et al. [11] put forward a nonlinear softening function to describe the constitutive relation, sometimes consistent with the test data:

$$\sigma = f_t \left\{ \left[1 + \left(\frac{c_1 \omega}{\omega_f} \right)^3 \right] \exp\left(-\frac{c_2 \omega}{\omega_f} \right) - \frac{\omega}{\omega_f} \left(1 + c_1^3 \right) \exp\left(-c_2 \right) \right\}, \tag{7}$$

where σ is the axial stress, f_t is the axial tensile strength, ω_f is the maximum crack width, ω is the crack width. c_1 and c_2 are the material parameters and test data are substituted into the model function and least squares fit optimization.

The axial-stress-crack-width curves are fitted by the above nonlinear softening function Equation (7), as shown in Figure 7(a). In this trial study, this tensile softening

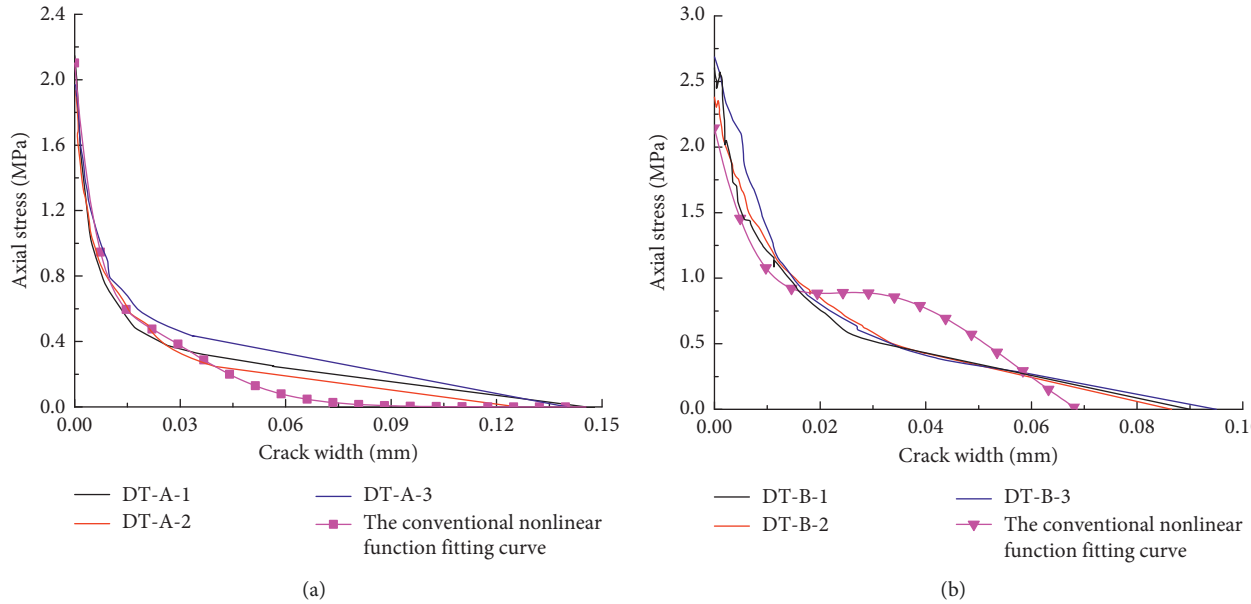

Figure 7: The result comparison of experimental and fitting curve of conventional nonlinear function. (a) 10^{-6} s^{-1}; (b) 10^{-5} s^{-1}.

function can reflect the tensile strength, the crack width, and the downward trend of the rock-mortar interface more accurately when the strain rate is 10^{-6} s^{-1}: $c_1 = 8.156$, $c_2 = 16.653$, $f_t = 2.041$, and $\omega_f = 0.141$.

3.2. A New Function of Containing Rate Effect. The softening nonlinear function fitting results using Equation (7); the fitting function mentioned by Reinhardt might be curvilinear oscillations in some situations. For instance, when the strain rate is 10^{-5} s^{-1}, two extreme points appear in the fitting result as shown in Figure 7(b), which obviously no longer meet the actual. This is because of the cubic term in the Reinhardt function, which has rich dynamic behaviors in control function equation, and may lead to situations with unstable and local bifurcation fitting curve solutions. Guo et al. studied the stability of a nonlinear dynamical system with cubical terms, and similar results were obtained [14].

At present, functions describing the FCM mainly include several forms, such as linear, bilinear, trilinear, exponential and power functions, among others. The linear function description is not accurate enough, and the bilinear and trilinear functions contain too many parameters and are complicated. In response to this problem, we use a new function that combines the power function and exponential functions as Equation (8) shows, based on the previous work, to describe the constitutive relation of the rock-mortar interface softening under different tension strain rates. This function can be more accurate in reflecting the tensile strength, crack width, and the downward trend of the rock-mortar interface, and the fitting results using it are shown in Figures 8(a)–8(c):

$$\sigma_n = c_1 f_t \left[\left(\exp\frac{-c_2\omega}{\omega_f}\right) + \left(1 - \frac{c_3\omega}{\omega_f}\right)^{1/5}\right], \quad (8)$$

where σ_n is the axial stress, f_t is the axial tensile strength, ω_f is the maximum crack width, ω is the crack width, and c_1, c_2, and c_3 are the material parameters, fitted by test data. The values of the parameters are shown in Table 2.

The new function successfully solves the problem of the inaccuracy of the description of the damage-evolution process of the rock-mortar interface. It can more accurately reflect the interface axial tensile strength, fracture width, and interface strength, and accordingly it can describe more accurately the constitutive relation of the rock-mortar interface softening under different strain rates.

From Table 1 and Figure 8, it can be seen that the physical and mechanical properties of the rock-mortar interface is sensitive to the change of the strain rate. With increasing of the strain rate from 10^{-6} s^{-1} to 10^{-4} s^{-1}, the axial tensile strength of the interface increases gradually, the width of cracks and the nonlinear degree of curves gradually reduce, and the concave trend of the curves changes to linear diminishing trend. This is because under low strain rate, only those cracks that can be activated under low stress level are fully extended and the extension and polymerization of those cracks lead to destruction of the sample before the stress reaches the level that can make the other cracks extend. From the macroscopic view, the crack develops and breaks along the weakest path of the interface of rock-mortar, as shown in Figures 9(b) and 9(d). Therefore, the specimen has lower stress strength and larger crack width. The rate effect loading test of granite by Liao et al. [15] and the test results of the mortar-granite interface by Wang et al. all got the same or similar conclusions [4]. With the increase of the strain rate, these cracks that can be excited at low stress levels have not yet fully expanded and polymerized, the crack that can only appear under high stress level has

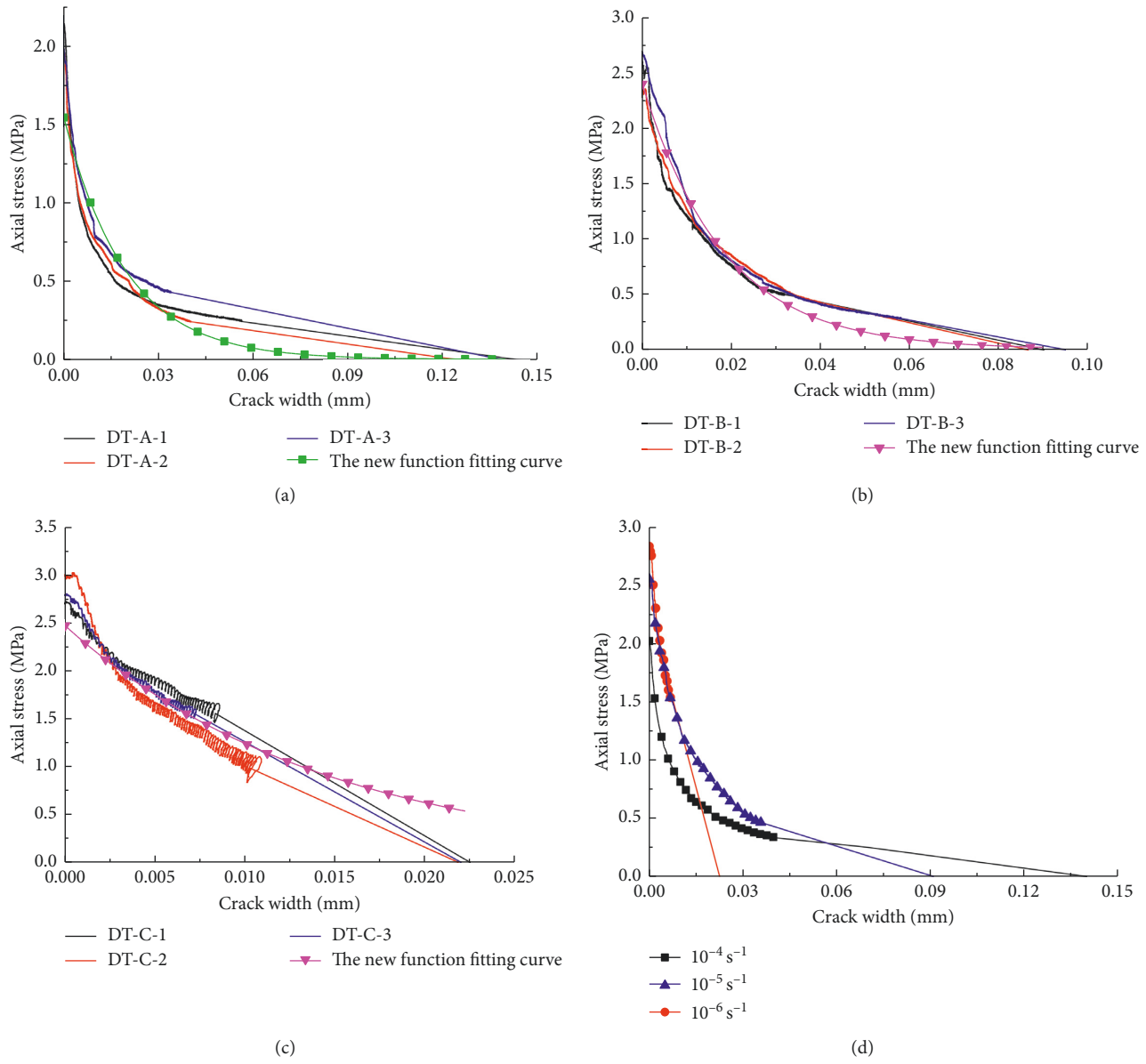

Figure 8: The result comparison of experimental and fitting curve of new function. (a) 10^{-6} s^{-1}; (b) 10^{-5} s^{-1}; (c) 10^{-4} s^{-1}; (d) the average curve of test.

Table 2: Equation parameters of the fitting curve of new function and fracture energy.

Strain rate (s^{-1})	f_t (MPa)	ω_f (mm)	c_1 (–)	c_2 (–)	c_3 (–)	Reduced chi-square (–)	Adjusted R-square (–)
10^{-6}	2.011	0.141	0.76	7.14	1	0.0131	0.903
10^{-5}	2.560	0.091	0.84	4.93	1	0.010	0.958
10^{-4}	2. 891	0.022	0.88	1.57	1	0.004	0.972

already been activated, extended, and aggregated. The crack extends along the shortest distance (the maximum energy consumption surface), making the section more smooth at the macrolevel. The possibility that cracks pass through the specimen's higher strength area will increase. Figures 9(c) and 9(e) show that some cracks occurred inside the mortar under higher strain rate, the strength of the specimen is relatively high, and the crack width is smaller. Using granite, Wang et al. studied the mechanical properties of soft rocks under dynamic axial tension and compression, which got similar results [4].

4. Conclusion

This paper explored the constitutive relation of rock-mortar interface softening at different strain rates by

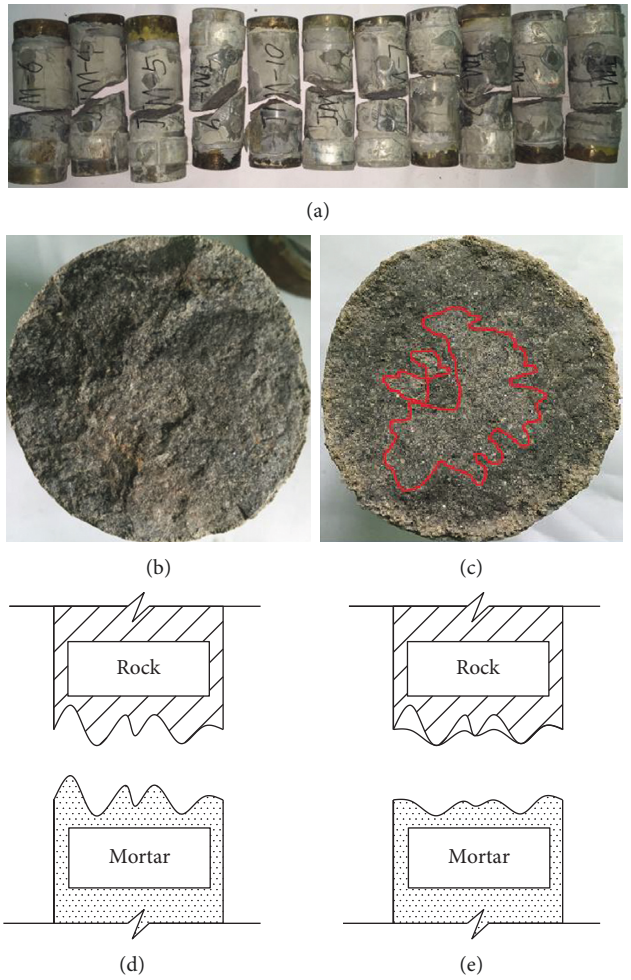

Figure 9: Sectional shape under different strain rates. (a) After damage of rock-mortar-interface specimens; cross sections of strain rates (b) 10^{-6} s^{-1} and (c) 10^{-4} s^{-1}; and schematic cross sections of strain rates (d) 10^{-6} s^{-1} and (e) 10^{-4} s^{-1}.

conducting direct axial tensile tests under three different such rates, 10^{-6}, 10^{-5}, and 10^{-4} s^{-1}, and the main conclusions are shown as follows:

(1) The rock-mortar interface tensile strength is sensitive to strain rate, and the relationship is that the higher the strain rate is, the higher the interface tensile strength goes. When the strain rate increases from 10^{-6} to 10^{-4} s^{-1}, the mean interface tensile strength increased by 55%.

(2) As the strain rate increases, the curvature of the axial-stress-deformation curve after the peak decreases, an effect that is more obvious with higher strain rates. The final crack width of the axial-stress-crack-width curve also decreases when the strain rate increases.

(3) In view of the traditional nonlinear softening function being prone to curve oscillation, the damage-evolution process of the rock-mortar interface cannot describe accurately. Thus, in this paper, a new tensile softening function is proposed, that is, $\sigma_n = c_1 f_t[(\exp(-c_2\omega/\omega_f)) + (1 - (c_3\omega/\omega_f))^{1/5}]$, which can more accurately reflect the tensile strength, crack width, and downward trend of the rock-mortar interface.

Data Availability

The introduction data supporting this manuscript are from previously reported studies and datasets, which have been cited. The processed data are available from the corresponding author upon request. The test raw data used to support the findings of this study are available from the corresponding author upon request. The analyzed data used to support the findings of this study are included within the article.

Conflicts of Interest

The authors declare that they have no conflicts of interest.

Acknowledgments

The authors are grateful to the Fundamental Research Funds for the Central Universities (Grant no. 2015B35214), the National Program on Key Basic Research Project (973 Program) (Grant no. 2015CB057903), and the National Natural Science Foundation of China (Grant no. 51379065) for financial support.

References

[1] T. Nonaka, R. J. Clifton, and T. Okazaki, "Longitudinal elastic wave in columns due to earthquake motion," *International Journal of Impact Engineering*, vol. 18, no. 7, pp. 889–898, 1996.

[2] S. Wolinski, A. D. Hordijk, H. W. Reinhardt, and H. A. W. Cornelissen, "Influence of aggregate size on fracture mechanics of parameters of concrete," *International Journal of Cement Composites and Lightweight Concrete*, vol. 9, no. 2, pp. 95–103, 1987.

[3] D. V. Phillips and Z. Binsheng, "Direct tension tests on notched and unnotched plain concrete specimens," *Magazine of Concrete Research*, vol. 45, no. 162, pp. 25–32, 1993.

[4] Y. Wang, S. X. Wu, J. K. Zhou, and D. Shen, "Experimental study of dynamic axial tensile mechanical properties of mortar-granite interface," *Rock and Soil Mechanics*, vol. 33, no. 5, pp. 1326–1332, 2012.

[5] F. Yan, X. T. Feng, R. Chen, K. Xia, and C. Jin, "Dynamic tensile failure of the rock interface between tuff and basalt," *Rock Mechanics and Rock Engineering*, vol. 45, no. 3, pp. 341–348, 2012.

[6] F. Dai and K. W. Xia, "Loading rate dependence of tensile strength anisotropy of Barre granite," *Pure and Applied Geophysics*, vol. 167, no. 11, pp. 1419–1432, 2010.

[7] D. Asprone, E. Cadoni, A. Prota, and G. Manfredi, "Dynamic behavior of a Mediterranean natural stone under tensile loading," *International Journal of Rock Mechanics and Mining Sciences*, vol. 46, no. 3, pp. 514–520, 2009.

[8] Q. H. Qian, C. Z. Qi, and M. Y. Wang, "Dynamic strength of rocks and physical nature of rock strength," *Journal of Rock Mechanics and Geotechnical Engineering*, vol. 1, no. 1, pp. 1–10, 2009.

[9] X. B. Li, Z. L. Zhou, F. J. Zhao et al., "Mechanical properties of rock under coupled static-dynamic loads," *Journal of Rock Mechanics and Geotechnical Engineering*, vol. 1, no. 1, pp. 31–40, 2009.

[10] A. Hillerborg, M. Modéer, and P. E. Petersson, "Analysis of crack formation and crack growth in concrete by means of fracture mechanics and finite elements," *Cement and Concrete Research*, vol. 6, no. 6, pp. 773–781, 1976.

[11] H. W. Reinhardt, H. A. W. Cornelissen, and D. A. Hordijk, "Tensile tests and failure analysis of concrete," *Journal of Structural Engineering*, vol. 112, no. 11, pp. 2462–2477, 1986.

[12] Y. Wang, S. X. Wu, J. K. Zhou et al., "Experimental study of dynamic axial tensile mechanical properties of granite," *Chinese Journal of Rock Mechanics and Engineering*, vol. 29, no. 11, pp. 2328–2336, 2010.

[13] S. X. Wu, Y. Wang, J. K. Zhou et al., "Experimental study of dynamic axial tensile constitutive relationship for mortar," *China Civil Engineering Journal*, vol. 1, pp. 13–22, 2012.

[14] J. B. Guo, G. S. Gao, and S. P. Yang, "Stability analysis of a non-linear dynamical system with cubical terms," *Journal of Shijiazhuang Railway Institute*, vol. 2, pp. 14–18, 2004.

[15] Z. Y. Liao, J. B. Zhu, K. W. Xia, and C. A. Tang, "Determination of dynamic compressive and tensile behavior of rocks from numerical tests of split Hopkinson pressure and tension bars," *Rock Mechanics and Rock Engineering*, vol. 49, no. 10, pp. 3917–3934, 2016.